

# Sites of Rupture in Human Atherosclerotic Carotid Plaques Are Associated With High Structural Stresses

## An In Vivo MRI-Based 3D Fluid-Structure Interaction Study

Dalin Tang, PhD; Zhongzhao Teng, PhD; Gador Canton, PhD; Chun Yang, MS; Marina Ferguson, BS; Xueying Huang, PhD; Jie Zheng, PhD; Pamela K. Woodard, MD; Chun Yuan, PhD

**Background and Purpose**—It has been hypothesized that high structural stress in atherosclerotic plaques at critical sites may contribute to plaque disruption. To test that hypothesis, 3D fluid-structure interaction models were constructed based on in vivo MRI data of human atherosclerotic carotid plaques to assess structural stress behaviors of plaques with and without rupture.

**Methods**—In vivo MRI data of carotid plaques from 12 patients scheduled for endarterectomy were acquired for model reconstruction. Histology confirmed that 5 of the 12 plaques had rupture. Plaque wall stress (PWS) and flow maximum shear stress were extracted from all nodal points on the lumen surface of each plaque for analysis. A critical PWS (maximum of PWS values from all possible vulnerable sites) was determined for each plaque.

**Results**—Mean PWS from all ulcer nodes in ruptured plaques was 86% higher than that from all nonulcer nodes (123.0 versus 66.3 kPa,  $P < 0.0001$ ). Mean flow maximum shear stress from all ulcer nodes in ruptured plaques was 170% higher than that from all nonulcer nodes (38.9 versus 14.4 dyn/cm<sup>2</sup>,  $P < 0.0001$ ). Mean critical PWS from the 5 ruptured plaques was 126% higher than that from the 7 nonruptured ones (247.3 versus 108 kPa,  $P = 0.0016$  using log transformation).

**Conclusion**—The results of this study show that plaques with prior ruptures are associated with higher critical stress conditions, both at ulcer sites and when compared with nonruptured plaques. With further validations, plaque stress analysis may provide additional stress indicators helpful for image-based plaque vulnerability assessment. (*Stroke*. 2009;40:3258-3263.)

**Key Words:** carotid artery ■ atherosclerosis ■ MRI ■ plaque rupture ■ fluid structure interaction

Atherosclerotic plaque vulnerability assessment and the ability to predict possible future plaque rupture are of vital importance for early diagnosis, prevention, and treatment of cardiovascular disease. It has been hypothesized that critical stress conditions (maximum principal stress values at critical sites where rupture is likely to occur) in the plaque may be closely related to plaque rupture and can be combined with current image-based assessment techniques for more accurate plaque evaluation and vulnerability assessment.<sup>1-2</sup> A major challenge for all available plaque assessment schemes is the lack of realistic lesion information based on in vivo patient data where both ruptured and nonruptured plaques are compared and analyzed. In vivo patient image data showing rupture verified by histological information provided by excised specimens could help to establish an in vivo benchmark for image-based or stress-based assessment schemes.

Currently, screening and diagnosis of patients with atherosclerotic plaques is based on medical images such as magnetic resonance image (MRI), ultrasound, intravascular ultra-

sound (IVUS), and computerized tomography (CT). In particular, MRI techniques have been shown to be able to noninvasively characterize plaque morphology and composition, and in particular, to identify fibrous cap rupture.<sup>3-12</sup> Chu et al performed serial high-spatial resolution, multisequence MRI studies identifying fibrous cap rupture, and a penetrating ulcer into carotid atherosclerotic plaque.<sup>10</sup>

In addition to plaque morphology, mechanical forces, considered to be potential rupture triggers, and plaque composition are key factors in the rupture process and should be considered in an integrated way for plaque assessment.<sup>12</sup> It has been hypothesized that image-based computational fluid-structure interaction (FSI) models with accurate stress and flow information may have potential to improve the current histology- and image-based plaque assessment schemes.<sup>1-2</sup> MRI-based computational simulations for plaque rupture investigation and vulnerability assessment have been conducted by several groups with interesting and significant results reported.<sup>13-26</sup> Steinman et al investigated effects of

Received May 23, 2009; accepted June 9, 2009.

From the Mathematical Sciences Department (D.T., Z.T., X.H.), Worcester Polytechnic Institute, Mass; the Department of Radiology (G.C., M.F., C.Y.), University of Washington, Seattle; the School of Mathematics (C.Y.), Beijing Normal University, China; and Mallinckrodt Institute of Radiology (J.Z., P.K.W.), Washington University, St. Louis, Mo.

Correspondence to Dalin Tang, Mathematical Sciences Department, Worcester Polytechnic Institute, Worcester, MA 01609. E-mail dtang@wpi.edu  
© 2009 American Heart Association, Inc.

*Stroke* is available at <http://stroke.ahajournals.org>

DOI: 10.1161/STROKEAHA.109.558676

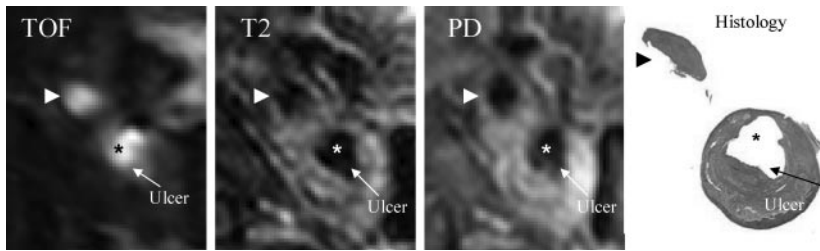


**Figure 1.** A human carotid plaque sample with corresponding TOF, T2-, and PD-weighted MR and histological images showing an ulcerated surface with thrombus (white arrow). \* indicates the internal carotid arterial lumen. The arrowhead indicates the external carotid artery.

plaque geometric features on flow behaviors using realistic plaque geometries.<sup>13–14</sup> Holzapfel et al introduced multi-layer anisotropic plaque models and showed that stress predictions from their models could be different from single-layer isotropic models by 50% to 200% or more.<sup>15–16</sup> Lee et al and Loree et al studied effects of plaque cap thickness and material properties on stress level and plaque rupture.<sup>17–18</sup> Vengrenyuk and Weinbaum et al demonstrated that plaque cap with microcalcification inclusions are associated with elevated stress levels and may be related to plaque rupture.<sup>19–20</sup> Influence of curvature dynamics and cyclic bending on coronary plaque stress and flow behaviors was investigated by Prosi et al and Tang et al.<sup>21–22</sup> Li et al performed structure analysis based on in vivo MRI of carotid arteries and found that wall stress was higher in symptomatic patients than in asymptomatic patients.<sup>23</sup> Groen and Wentzel et al in a case report indicated that plaque rupture in the carotid artery was localized at the high shear stress region.<sup>24</sup> In the introduction of image-based FSI models, Tang et al demonstrated that fluid-structure interactions, axial stretch, cyclic bending, and a preshrink process for in vivo imaged-based models have considerable effects on accuracy of stress/strain predictions.<sup>1–2,22,25–26</sup>

To date, evidence from 3D FSI models based on in vivo MRI data of ruptured human atherosclerotic carotid plaques linking plaque rupture to corresponding stress and flow shear stress conditions is still lacking in the current literature because of the difficulties in obtaining in vivo MRI data with indication of plaque ruptures and constructing 3D FSI models. In this study, 3D computational multi-component models with FSI were constructed based on in vivo MRI data of carotid plaques acquired from 12 patients with advanced lesions. Disruption of the plaque surface considered in this article was defined as the presence of ulcerated regions in the MR images. We evaluated plaque wall maximum principal stress (PWS) and flow maximum shear stress (FMSS) values on all lumen surface nodal points to study the associations between mechanical stress and flow shear stress conditions and plaque rupture sites.

## Methods

### MRI Data Acquisition

3D in vivo MR images of human atherosclerotic carotid plaques from 12 patients scheduled for carotid endarterectomy (age: 54 to 82, mean=68, 11M, 1F; 5 plaques with ulcerations which are indication of prior ruptures, 7 plaques without prior rupture) were acquired before the surgery at the University of Washington, Seattle (n=11) and Washington University, St. Louis (n=1), and after informed consent. The institutional review boards of each institution approved the consent forms and study protocols. Patients were imaged with a

1.5-T MR scanner (Signa Horizon EchoSpeed, General Electric Health Care). Precontrast MR images included double-inversion-recovery T1-, proton density-, and T2-weighted (T1W, PDW, and T2W; respectively), and time-of-flight (TOF). Postcontrast double-inversion recovery T1W MR images of carotid arteries were obtained with a previously published standardized protocol (T1W: repetition time/echo time/inversion time, 800/10/650 ms; PDW and T2W: repetition time/echo time, 3RR, 20/40 ms; TOF: repetition time/echo time, 23/3.8 ms).<sup>7–10</sup> A gadolinium-based contrast agent (Omniscan, Amersham Health), 0.1 mmol/kg (0.2 mL/kg) body weight, was injected intravenously with a power injector, and acquisition of postcontrast T1W images occurred 6 to 10 minutes after injection. All images were obtained with the following parameters: 16 cm field-of-view, 256×256 matrix size, and 2-mm slice thickness. After interpolation, the in-plane resolution is 0.31×0.31 mm<sup>2</sup>. The longitudinal coverage covered the bulk region of each carotid lesion.

MR images were segmented using custom made analysis tools (CASCADE<sup>27</sup> developed at the Vascular Imaging Laboratory at University of Washington, and APIA, from Washington University) to identify lipid-rich necrotic core, loose matrix, calcification, thrombus, hemorrhage, and the presence or absence of ulcer, as the indicator of disruption.<sup>4–5,7–8,10</sup> Disruption was confirmed by the histology after matching to the MR images.<sup>9</sup> The histology-validated MRI analysis of the status of the fibrous cap resulted in 5 arteries with ulcerated plaques. Figure 1 shows a plaque slice with TOF, T1-, and PD-weighted MR and histological images showing an ulcer. Figure 2 gives a set of 10 slices of PD-weighted MR images and segmented contour plots showing 3D reconstruction process.

### 3D Reconstruction, Shrink-Stretch Process, and Mesh Generation Process

Under the in vivo condition, the artery is axially stretched and pressurized, thus axial and circumferential shrinking was applied a priori to generate the start-shape for the computational simulation. The shrinkage in axial direction was 9% so that the vessel would regain its in vivo length with a 10% axial stretch. Circumferential shrinkage for lumen and outer wall was determined so that: (1) total mass volume was conserved; (2) plaque geometry after 10% axial stretch and pressurization had the best match with the original in vivo geometry. Because advanced plaques have complex irregular geometries with component inclusions that are challenging for mesh generation, a component-fitting mesh generation technique was developed to generate mesh for these models. Using this technique, the 3D plaque domain was divided into hundreds of small “volumes” to curve-fit the irregular plaque geometry with plaque component inclusions.<sup>22</sup> Ulcers were replaced with lipid cores covered by a thin cap. This is our best approximation for the prerupture geometry of these plaque samples. 3D surfaces, volumes, and computational mesh were created with ADINA (ADINA R&D, Inc) computing environment. Each plaque model required about 3600 small volumes to be created to fit the shape of wall and adjacent components, and about 1000 small volumes were needed for the corresponding fluid domain.

### FSI Computational Model

Both the artery wall and plaque components were assumed to be hyperelastic, isotropic, incompressible, and homogeneous. Blood flow was assumed to be laminar, Newtonian, viscous, and incompressible. The incompressible Navier-Stokes equations with arbitrary Lagrangian-Eulerian (ALE) formulation were used as the governing

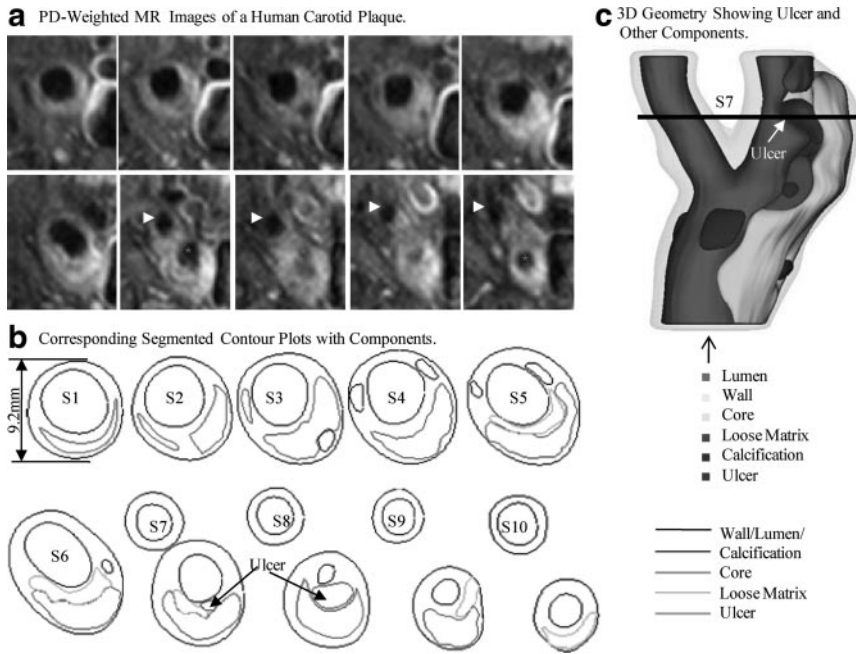


**Figure 2.** PD-weighted MR images and segmented contour plots showing the 3D reconstruction process.

equations. A no-slip condition between all interfaces was assumed. Patient-specific systolic and diastolic pressure conditions from the last hospital admission were used to impose pulsatile pressure conditions at the inlet and outlet of the artery. The modified Mooney-Rivlin model was used to describe the material property of each component in the plaque,<sup>25–26,28</sup>

$$W = c_1 (I_1 - 3) + c_2 (I_2 - 3) + D_1 [\exp(D_2 (I_1 - 3)) - 1], \quad (1)$$

where  $I_1 = \sum C_{ii}$ ,  $I_2 = \frac{1}{2} [I_1^2 - C_{ij}C_{ij}]$  are the first and second strain invariants,  $C = [C_{ij}] = X^T X$  is the right Cauchy-Green deformation tensor,  $X = [X_{ij}] = [\partial x_i / \partial a_j]$ ,  $\{x_i\}$  is current position,  $\{a_i\}$  is original position,  $c_1$  and  $D_1$  are material parameters chosen to match experimental measurement.<sup>25–26</sup> In this article, the following parameter values were chosen: vessel/fibrous cap,  $c_1 = 36.8 \text{ kPa}$ ,  $D_1 = 14.4 \text{ kPa}$ ,  $D_2 = 2$ ; calcification,  $c_1 = 368 \text{ kPa}$ ,  $D_1 = 144 \text{ kPa}$ ,  $D_2 = 2.0$ ; lipid core/hemorrhage/ulcers,  $c_1 = 2 \text{ kPa}$ ,  $D_1 = 2 \text{ kPa}$ ,  $D_2 = 1.5$ ; loose matrix,  $c_1 = 18.4 \text{ kPa}$ ,  $D_1 = 7.2 \text{ kPa}$ ;  $D_2 = 1.5$ .  $c_2 = 0$  was set for all materials.

### Solution Method

The coupled FSI plaque models were solved by a commercial finite-element package ADINA. This software uses unstructured finite element methods for both fluid and solid models. Nonlinear incremental iterative procedures were used to handle fluid-structure interactions. The governing finite element equations for both the solid and fluid models were solved by the Newton-Raphson iteration method. Details of the models and methods are given in Tang et al<sup>25–26</sup> and Bathe.<sup>28</sup>

### Plaque Stress/Strain and Flow Shear Stress Data Extraction

Data for PWS and FMSS were extracted from 3D FSI solutions for all integral nodes (total nodes: structure=7028; fluid=6418) on lumen surfaces of 12 plaque models for analysis. Each node was assigned a node type (lipid, calcification, ulcer, loose matrix, and wall) if the node was not covering any component) according to its location and nearby component. Mean values of PWS, PWSN, and FMSS for each node type from each patient were calculated for analysis and comparisons. A *t* test ( $P < 0.05$ ) was used to determine whether there was a significant difference between the data compared.

Using previously published critical site selection method and critical stress approach,<sup>2</sup> a critical PWS (CPWS) is determined for each plaque. CPWS was defined as the maximum of PWS values from all possible vulnerable sites which included sites with local

stress concentration (local maximum), especially where a thin cap was covering a plaque component, but excluded healthy sites where rupture is unlikely, even if a local stress maximum occurred there.

### Results

Figure 3 gives an overview of solution features from 3D FSI models using the plaque sample given in Figure 2. Maximum principal stress (Stress- $P_1$ ) on stacked cross-section slices, a bifurcation cut (B-cut) surface, and a cross-section cut (at S7 location) were plotted showing the site of rupture. Maximum Stress- $P_1$  was observed at the site of rupture. To analyze mechanical conditions (structural stress and flow shear stress) on the lumen surface corresponding to different tissue types and to identify differences between ulcer and nonulcer nodes, data were extracted from the full 3D FSI solutions and mean values of PWS and FMSS of ulcer, lipid core, calcification, wall, and all nonulcer nodes are summarized in Tables 1 and 2. kPa and  $\text{dyn/cm}^2$  were used as the units for PWS and FMSS, respectively ( $1 \text{ kPa} = 10^4 \text{ dyn/cm}^2$ ).

### Ulcer Nodes Are Associated With Higher PWS Values Compared to Nonulcer Nodes

For the 5 plaques with ulcers, the mean PWS value from all ulcer nodes was 123.0 kPa, which is 86% higher than the mean PWS value (66.3 kPa) from all nonulcer nodes ( $P < 0.0001$ ). The differences between the individual mean PWS values from ulcer and nonulcer nodes for each of the 5 plaque samples were also statistically significant. Excluding the ulcer nodes, the differences between the mean PWS values from lipid, wall, and all nonulcer nodes are modest (<5%).

### Overall Results Showing Ulcer Nodes Are Associated With Higher FMSS

Table 2 indicates that mean FMSS from all ulcer nodes ( $38.9 \text{ dyn/cm}^2$ ) was 170% higher than that ( $14.4 \text{ dyn/cm}^2$ ) from all nonulcer nodes for the 5 plaques with ulcerations. Individual plaque mean FMSS data showed mixed results. Three plaques



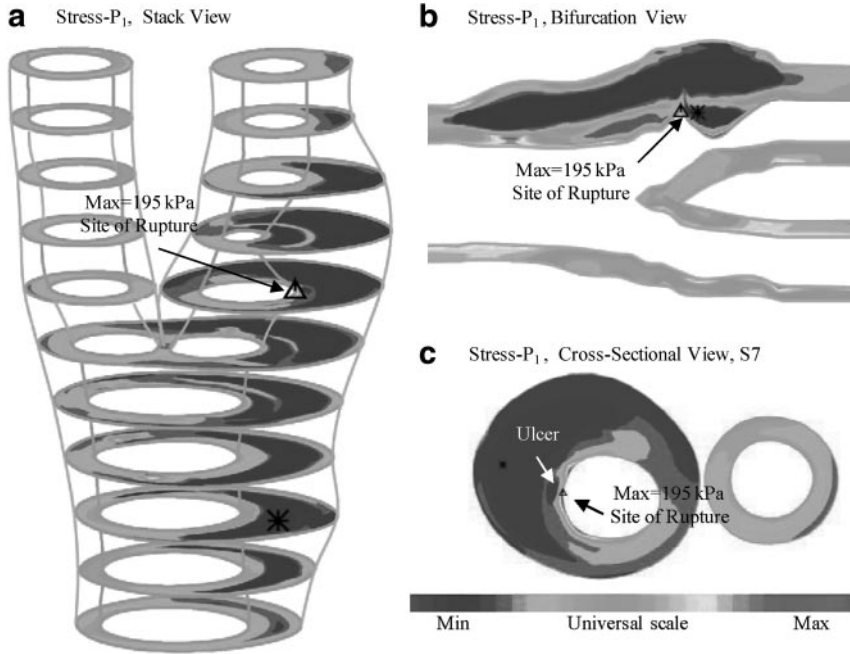


**Figure 3.** 3D plaque wall stress plots showing maximum critical stress at the ulcer site of ulcerated artery sample shown in Figures 1 and 2.

showed mean FMSS values on ulcer nodes were greater than those on nonulcer nodes (23.6, 49.0, 54.7) versus (16.2, 9.90, 7.13),  $P < 0.0001$ ; one plaque showed mean FMSS (10.8) on ulcer nodes was less than mean FMSS (18.0) on nonulcer nodes ( $P < 0.0001$ ); another plaque showed mean FMSS (39.3) was greater than that (34.1) on nonulcer nodes, but the difference was not statistically significant ( $P = 0.6848$ ).

**Comparison of Plaques With Ruptures (n=5) and Plaques Without Rupture (n=7)**

Tables 1 and 2 list mean values of PWS and FMSS of the 2 groups of plaques on different node types; all nodes com-

bined; and all nonulcer nodes combined. Excluding the ulcer nodes, differences of those mean values between the ruptured and nonruptured groups are not significant.

**Critical Stress Values From Plaques With Rupture Were Significantly Higher Than Those from Nonruptured Plaques**

CPWS values from the 5 plaques with rupture were (unit: kPa): 457.85, 241.90, 195.51, 161.92, and 179.14 with an average =  $247.3 \pm 121.4$ . CPWS values from the 7 nonruptured plaques were: 81.68, 129.31, 103.68, 143.70, 94.32, 102.88, and 108.03 with average =  $109.1 \pm 21.0$ . The average CPWS from the

**Table 1. Summary of Mean Plaque Wall Stress (PWS) Values of Ulcer, Lipid Core, Calcification, Wall, All Nodes, and All Nonulcer Nodes for the 12 Plaque Samples**

Case	Ulcer		Wall		Lipid		Calcification		All Nodes		All Nonulcer		P Value
	Mean	n	Mean	n	Mean	n	Mean	n	Mean	n	Mean	n	
P1	157.8	18	73.3	110	99.8	65			90.1	193	83.1	175	<0.0001
P2	87.3	116	71.7	410	60.0	15	30.4	23	70.5	626	66.7	510	<0.0001
P3	141.6	7	62.3	431	59.0	167	60.0	16	62.3	621	61.4	614	0.0237
P4	104.5	28	70.6	428	76.2	182	50.6	33	74.3	772	73.1	744	0.0008
P5	164.1	95	72.0	537	59.2	87			82.7	719	70.3	624	<0.0001
All 5 Rup	123.0	264	69.5	1916	70.3	516	46.2	72	74.0	2931	66.3	2667	
P6			33.8	276	35.4	147			35.0	442	35.0	442	
P7			74.6	393	79.0	114	45.2	15	74.2	531	74.2	531	
P8			57.0	426	74.6	73			59.6	499	59.6	499	
P9			71.0	440	80.6	83			72.6	523	72.6	523	
P10			63.7	424	70.0	130			65.2	554	65.2	554	
P11			77.2	743	49.6	226			70.8	969	70.8	969	
P12			60.0	484	64.5	95			60.7	579	60.7	579	
7 No Rup			65.2	3186	60.8	868	45.2	15	64.1	4097	64.1	4097	
All 12 P	123.0	264	66.8	5102	64.3	1384	46.0	87	68.0	7028	66.1	6764	<0.0001

n indicates number of nodes.

The P values are for the ulcer vs nonulcer comparisons. Unit for PWS: kPa.

**Table 2. Summary of Mean Flow Maximum Shear Stress (FMSS) Values of Ulcer, Lipid Core, Calcification, Wall, All Nodes, and All Nonulcer Nodes for the 12 Plaque Samples**

Case	Ulcer		Wall		Lipid		Calcification		All Nodes		All Nonulcer		P Value
	Mean	n	Mean	n	Mean	n	Mean	n	Mean	n	Mean	n	
P1	39.3	5	30.6	109	42.4	46			34.2	160	34.1	155	0.6848
P2	54.7	89	8.7	260	2.5	10	1.0	16	17.3	416	7.1	327	<0.0001
P3	23.6	6	13.9	431	22.4	170	11.8	15	16.3	622	16.2	616	<0.0001
P4	49.0	27	12.8	425	6.5	181	7.2	30	11.3	764	9.9	737	<0.0001
P5	10.8	57	14.6	362	41.2	53			17.1	472	18.0	415	<0.0001
All 5 Rup	38.9	184	14.0	1587	19.9	460	6.7	61	16.2	2434	14.4	2250	
P6			7.3	229	8.2	110			7.5	350	7.5	350	
P7			11.9	307	25.6	105	7.8	8	15.1	426	15.1	426	
P8			11.1	426	13.3	73			11.4	499	11.4	499	
P9			11.4	448	9.0	83			11.0	531	11.0	531	
P10			7.4	435	9.6	130			7.9	565	7.9	565	
P11			59.4	1039	65.6	226			60.5	1265	60.5	1265	
P12			15.0	288	19.0	60			15.7	348	15.7	348	
7 No Rup			26.6	3172	28.6	787	7.8	8	26.9	3984	26.9	3984	
All 12 P	38.9	184	22.4	4759	25.4	1247	6.8	69	22.8	6418	22.4	6234	<0.0001

n indicates number of nodes.

P values are for ulcer vs nonulcer comparisons. Unit for FMSS: dyn/cm<sup>2</sup>.

5 ruptured cases was 126% higher than that from the 7 nonruptured cases ( $P=0.0016$  using log transformation).

## Discussion

### In Vivo Evidence Linking Localized Stress Conditions to Plaque Vulnerability

This is the first study with a relative large in vivo patient data in a mechanical analysis. The results showed evidence that high plaque stresses are indeed linked to sites of plaque rupture. The lesions studied were all advanced complex plaques, 5 of them having an ulcerated surface. Evidence linking local critical stress conditions with actual plaque rupture sites based on in vivo data are of great importance in establishing the bench mark for atherosclerotic plaque mechanical assessment.<sup>2</sup>

### The Role of Flow Shear Stress in Plaque Rupture Process

Numerous studies have attempted to determine a solid link between flow shear stress and plaque progression and rupture. Groen and Wentzel et al reported a follow-up case study showing high flow shear stress region was associated with site of plaque rupture.<sup>24</sup> The overall results from this study are supporting their findings. Individual differences suggest that larger-scale study is needed to further clarify the role of FMSS in the rupture process. Considering that critical structural stress is at about 100 to 400 kPa level and FMSS is only at <10 Pa, contribution from flow shear stress acting as a rupture trigger may be much smaller than that from structural stress. However, high flow shear stress may act on the lumen surface in a long-term process leading to endothelial dysfunction and lumen surface weakening.

### Limitations

The models used in the study made use of patient-specific plaque morphology and systolic/diastolic pressure conditions with the intent for potential patient-screening applications. However, the models lack patient-specific vessel and plaque component material properties because of an inability to measure these material properties in vivo using the current imaging format. Accurate anisotropic vessel and plaque component material property measurements will improve the model predictions. The accuracy of the computational models when compared to histology is also compromised by the limited in vivo MRI resolution ( $0.31 \times 0.31 \times 2.0$  mm<sup>3</sup>).

It is known that blood flow in carotid arteries with severe stenosis may become disturbed or even turbulent.<sup>29</sup> Although many flow and geometric parameters may affect flow behavior, considerable turbulence can be present when stenosis severity (based on the diameter measurement) exceeds 70%.<sup>29</sup> Stenosis severity (based on diameter) of the 12 plaques was <40% in 7 cases, <55% in 4 cases, <75% in one case. Although the choice of laminar flow model may be justified for this study, as only one case exceeded the stenosis degree that guarantees turbulent Reynolds number, a turbulent model will be considered in future studies for better predictions. Local disturbed flow behaviors were complex and may be reported in future studies.

### Conclusion

The results from 3D FSI models based on in vivo MRI data for human carotid plaques (5 with ruptures, 7 nonruptures) show that plaques with prior ruptures are associated with higher critical plaque wall stress conditions when compared with nonruptured plaques and that those high critical stress conditions occur at ulcer sites. These findings, when further validated in a

larger study, may provide additional stress indicators helpful for image-based plaque vulnerability assessment.

### Sources of Funding

This research was supported in part by NSF grant DMS-0540684 and NIH grant R01 EB004759.

### Disclosures

None.

### References

- Tang D, Yang C, Zheng J, Woodard PK, Sicard GA, Saffitz JE, Yuan C. 3D MRI-based multi-component FSI models for atherosclerotic plaques a 3-D FSI model. *Ann Biomed Eng.* 2004;32:947–960.
- Tang D, Yang C, Zheng J, Woodard PK, Saffitz JE, Petruccioli JD, Sicard GA, Yuan C. Local maximal stress hypothesis and computational plaque vulnerability index for atherosclerotic plaque assessment. *Ann Biomed Eng.* 2005;33:1789–1801.
- Carr S, Farb A, Pearce WH, Virmani R, Yao JS. Atherosclerotic plaque rupture in symptomatic carotid artery stenosis. *J Vasc Surg.* 1996;23:755–765.
- Hatsukami TS, Ross R, Polissar NL, Yuan C. Visualization of fibrous cap thickness and rupture in human atherosclerotic carotid plaque in vivo with high-resolution magnetic resonance imaging. *Circulation.* 2000;102:959–964.
- Yuan C, Mitsumori LM, Ferguson MS, Polissar NL, Echelard DE, Ortiz G, Small R, Davies JW, Kerwin WS, and Hatsukami TS. In vivo accuracy of multispectral MR imaging for identifying lipid-rich necrotic cores and intraplaque hemorrhage in advanced human carotid plaques. *Circulation.* 104:2051–2056, 2001.
- Wiesmann F, Robson MD, Francis J, Petersen SE, Leeson CP, Channon KM, Neubauer S. Images in cardiovascular medicine. Visualization of the ruptured plaque by magnetic resonance imaging. *Circulation.* 2003;108:2542.
- Yuan C, Mitsumori LM, Beach KW, Maravilla KR. Special review, Carotid atherosclerotic plaque: noninvasive MR characterization and identification of vulnerable lesions. *Radiology.* 2001;221:285–299.
- Saam T, Ferguson MS, Yarnykh VL, Takaya N, Xu D, Polissar NL, Hatsukami TS, Yuan C. Quantitative evaluation of carotid plaque composition by in vivo MRI. *Arterioscler Thromb Vasc Biol.* 2005;25:234–239.
- Mitsumori LM, Hatsukami TS, Ferguson MS, Kerwin WS, Cai J, Yuan C. In vivo accuracy of multisequence MR imaging for identifying unstable fibrous caps in advanced human carotid. *J Magn Reson Imag.* 2003;17:410–420.
- Chu B, Yuan C, Takaya N, Shewchuk JR, Clowes AW, Hatsukami TS. Images in cardiovascular medicine. Serial high-spatial-resolution, multi-sequence magnetic resonance imaging studies identify fibrous cap rupture and penetrating ulcer into carotid atherosclerotic plaque. *Circulation.* 2006;113:e660–e661.
- Cai JM, Hatsukami TS, Ferguson MS, Small R, Polissar NL, Yuan C. Classification of human carotid atherosclerotic lesions with in vivo multicontrast magnetic resonance imaging. *Circulation.* 2002;106:1368–1373.
- Fuster V. *The Vulnerable Atherosclerotic Plaque: Understanding, Identification, and Modification.* Fuster V, Cornhill JF, Dinsmore RE, Fallonm JT, Insull W, Libby P, Nissen S, Rosenfeld ME, Wagner WD, eds. AHA Monograph Series. Armonk, NY: Futura Publishing; 1998.
- Steinman DA, Thomas JB, Ladak HM, Milner JS, Rutt BK, Spence JD. Reconstruction of carotid bifurcation hemodynamics and wall thickness using computational fluid dynamics and MRI. *Magn Reson Med.* 2002;47:149–159.
- Steinman DA. Image-based computational fluid dynamics modeling in realistic arterial geometries. *Ann Biomed Eng.* 2002;30:483–497.
- Holzappel GA, Stadler M, Schulze-Bause CAJ. A layer-specific three-dimensional model for the simulation of balloon angioplasty using Magnetic Resonance Imaging and mechanical testing. *Ann Biomed Eng.* 2002;30:753–767.
- Holzappel GA, Sommer G, Regitnig P. Anisotropic mechanical properties of tissue components in human atherosclerotic plaques. *J Biomech Eng.* 2004;126:657–665.
- Lee RT, Schoen FJ, Loree HM, Lark MW, Libby P. Circumferential stress and matrix metalloproteinase 1 in human coronary atherosclerosis. Implications for plaque rupture. *Arterioscler Thromb Vasc Biol.* 1996;16:1070–1073.
- Loree HM, Kamm RD, Stringfellow RG, Lee RT. Effects of fibrous cap thickness on peak circumferential stress in model atherosclerotic vessels. *Circ Res.* 1992;71:850–858.
- Vengrenyuk Y, Cardoso L, Weinbaum S. Micro-CT based analysis of a new paradigm for vulnerable plaque rupture: cellular microcalcifications in fibrous caps. *Mol Cell Biomech.* 2008;5:37–47.
- Vengrenyuk Y, Carlier S, Xanthos S, Cardoso L, Ganatos P, Virmani R, Einav S, Gilchrist L, Weinbaum S. A hypothesis for vulnerable plaque rupture due to stress-induced debonding around cellular microcalcifications in thin fibrous caps. *Proc Natl Acad Sci U S A.* 2006;103:14678–14683.
- Prosi M, Perktold P, Ding Z, Friedman MH. Influence of curvature dynamics on pulsatile coronary artery flow in a realistic bifurcation model. *J Biomech.* 2004;37:1767–1775.
- Tang D, Yang C, Kobayashi S, Zheng J, Woodard PK, Teng Z, Billiri K, Bach R, Ku DN. 3D MRI-based anisotropic FSI models with cyclic bending for human coronary atherosclerotic plaque mechanical analysis. *J Biomech Engng.* In press.
- Li ZY, Howarth SP, Tang T, Graves MJ, U-King-Im J, Trivedi RA, KirkPatrick PJ, Gillard JH. Structural analysis and magnetic resonance imaging predict plaque vulnerability: a study comparing symptomatic and asymptomatic individuals. *J Vasc Surg.* 2007;45:768–775.
- Groen HC, Gijzen FJ, van der Lugt A, Ferguson MS, Hatsukami TS, van der Steen AF, Yuan C, Wentzel JJ. Plaque rupture in the carotid artery is localized at the high shear stress region: a case report. *Stroke.* 2007;38:2379–2381.
- Tang D, Yang C, Mondal S, Liu F, Canton G, Hatsukami TS, Yuan C. A Negative correlation between human carotid atherosclerotic plaque progression and plaque wall stress: in vivo MRI-based 2D/3D FSI models. *J Biomechanics.* 2008;41:727–736.
- Yang C, Tang D, Yuan C, Hatsukami TS, Zheng J, Woodard PK. In vivo/ex vivo MRI-based 3D models with fluid-structure interactions for human atherosclerotic plaques compared with fluid/wall-only models. *CMES: Computer Modeling in Engineering and Sciences.* 2007;19:233–245.
- Kerwin W, Xu D, Liu F, Saam T, Underhill H, Takaya N, Chu B, Hatsukami T, Yuan C. Magnetic resonance imaging of carotid atherosclerosis: Plaque analysis. *Topics Magn Reson Imaging.* 2007;18:371–378.
- Bathe KJ. *Theory and Modeling Guide*, Vol I: ADINA; Vol II: ADINA-F. Watertown, Mass: Adina R&D Inc; 2002.
- Ku DN. Blood flow in arteries. *Annu Re Fluid Mech.* 1997;29:399–434.

**Sites of Rupture in Human Atherosclerotic Carotid Plaques Are Associated With High Structural Stresses: An In Vivo MRI-Based 3D Fluid-Structure Interaction Study**  
Dalín Tang, Zhongzhao Teng, Gador Canton, Chun Yang, Marina Ferguson, Xueying Huang, Jie Zheng, Pamela K. Woodard and Chun Yuan

*Stroke*. 2009;40:3258-3263; originally published online July 23, 2009;  
doi: 10.1161/STROKEAHA.109.558676

*Stroke* is published by the American Heart Association, 7272 Greenville Avenue, Dallas, TX 75231  
Copyright © 2009 American Heart Association, Inc. All rights reserved.  
Print ISSN: 0039-2499. Online ISSN: 1524-4628

The online version of this article, along with updated information and services, is located on the World Wide Web at:

<http://stroke.ahajournals.org/content/40/10/3258>

**Permissions:** Requests for permissions to reproduce figures, tables, or portions of articles originally published in *Stroke* can be obtained via RightsLink, a service of the Copyright Clearance Center, not the Editorial Office. Once the online version of the published article for which permission is being requested is located, click Request Permissions in the middle column of the Web page under Services. Further information about this process is available in the [Permissions and Rights Question and Answer](#) document.

**Reprints:** Information about reprints can be found online at:  
<http://www.lww.com/reprints>

**Subscriptions:** Information about subscribing to *Stroke* is online at:  
<http://stroke.ahajournals.org/subscriptions/>